Electronic Supplementary Information

NiZn Double Hydroxide Nanosheet-Anchored Nitrogen-Doped Graphene Enriched with ϒ-NiOOH Phase as an Activity Modulated Water Oxidation Electrocatalyst

Ayasha Nadeema,[1,3] Vishal M. Dhavale,[2] Sreekumar Kurungot[*,1,3]

[1]*Physical and Materials Chemistry Division, CSIR-National Chemical Laboratory, Pune-411008, India,*

Fax: +91-20-25902636; Tel: +91-20-25902566;

E-mail: k.sreekumar@ncl.res.in

[3]*Academy of Scientific and Innovative Research (AcSIR), Anusandhan Bhawan, New Delhi-110001, India.*

[2]*Inorganic and Physical Chemistry Division, CSIR-Indian Institute of Chemical Technology, Hyderabad-500007, India.*

Content

1. Experimental:

1.1. Materials.

Nickel chloride hexahydrate [$NiCl_2.6H_2O$], zinc acetate dihydrate [$Zn(CH_3COO)_2.2H_2O$)], urea [$CO(NH_2)_2$], graphite, potassium permanganate ($KMnO_4$), melamine, hydrogen peroxide (H_2O_2), potassium hydroxide (KOH) were purchased from Sigma-Aldrich. Methanol, phosphoric acid (H_3PO_4) and sulphuric acid (H_2SO_4) were purchased from Thomas Baker. The entire chemical reagents were used as such without any further purification.

1.2. Synthesis of graphene oxide (GO) and reduced graphene oxide:

Graphene oxide (GO) was synthesized by following an improved Hummer's method[1] from natural graphite by giving it harsh oxidizing treatment. For the synthesis of reduced graphene oxide (rGO), GO flakes were kept into a quartz tube for annealing at 900 ^{o}C in a tubular furnace under argon atmosphere. For the required reduction of GO to rGO, the furnace temperature was maintained for 3 h. In the subsequent process, the furnace was cooled down naturally under the same atmosphere.

1.3. Synthesis of N-doped reduced graphene oxide (N-rGO):

1 g of graphene oxide (GO) was dissolved in adequate DI water by water-bath sonication and overnight stirring. Subsequently, melamine was added in the ratio of 1:5 into the GO-DI water solution and the mixture was continued for 24 h stirring, after that the mixture was heated at 80 ^{o}C with stirring until it was dried completely. The dried GO-melamine powder was subjected for heating at 900 ^{o}C for 3 h under argon atmosphere. Thereafter,

the furnace was allowed to cool down naturally in the same atmosphere and N-rGO was collected.

2. Structural Characterization:

The as synthesized samples were examined by Rigaku SmartLab X-ray diffractometer instrument using Cu-K_α radiation (λ =1.54Å) with a scan rate of 3^o min^{-1} in the 2θ range of 5 to 80^o. Morphological investigation, particle size analysis, and high resolution imaging were performed using FEI, TECNAI G2 F20 transmission electron microscopy (TEM) instrument (conditions: accelerated voltage = 200 kV, and resolution = 0.17 nm). The sample for TEM was prepared by drop coating the well dispersed sample in isopropyl alcohol (1 mg of sample in 5 ml solvent) on a carbon coated 200 mess copper grid. The sample coated TEM grid was dried under an IR-lamp prior to imaging. X-ray photoelectron spectroscopy (XPS) studies were performed using KRATOS NOVA, a highly automated X-ray photoelectron spectrometer. Thermal behaviour of samples was analysed using a SDT Q600 DSC-TDA thermo-gravimetric (TG) instrument in the temperature range of 20-900 ^{o}C at a heating rate of 10 ^{o}C min^{-1} in oxygen atmosphere. Raman spectral investigations were performed using 632 nm green laser (NRS 1500W) on a HR 800 RAMAN spectrometer. Elemental mapping and SEM images were obtained using FEI Nova NanoSEM 450 FE-SEM instrument. N_2 adsorption isotherm experiments were performed on a Quantachrome Quadrasorb automatic volumetric instrument to analyse surface area and pore volume of the samples. FTIR analysis was performed on Bruker Tensor 27 FT-IR instrument using OPUS Data Collection Program.

3. Electrochemical Studies:

The electrochemical data needed for the present work were acquired with the help of a set of electrochemical techniques including cyclic voltammetry (CV) and linear sweep voltammetry (LSV) using a rotating disc electrode (RDE) made of glassy carbon (0.0706 cm^2) and a rotating ring disk electrode (RRDE) with the help of Pine Instruments. A three-electrode electrochemical cell was used with a VMP3 model BioLogic potentiostat. A graphite rod (Alfa Aesar, 99.99%) was used as the counter electrode and Hg/HgO was employed as the reference electrode.

For OER activity comparison, we included the electrochemical activity of 20% RuO_2/C. We prepared RuO_2/C from commercial RuO_2 hydrate by adopting the procedure reported by Thomas Audichon *et al.*[2] The RuO_2 hydrate was calcined in a muffle furnace under air atmosphere to dehydrate the RuO_2 hydrate. For that, the temperature of the furnace was increased gradually to 400 °C by applying successively 1 h steps at 250, 350, and 400 °C with a heating rate of 2 °C min^{-1}. Afterward, the heat treated RuO_2 was mixed with Vulcan carbon in 1: 4 ratio to get 20% RuO_2/C.

For the working electrode preparation, firstly, the catalyst ink was prepared by mixing the electrocatalyst (5 mg) in 1 mL isopropyl alcohol-water (3:2) solution and 40 μL of Nafion solution (5 wt%, Sigma-Aldrich) using water-bath sonication for approximately 1 h. Meanwhile, the RDE and RRDE electrode surfaces were polished with 0.3 μm alumina slurry in DI-water followed by cleaning with DI-water and acetone. 2.5 μL of the ink (final loading of catalyst = 0.18 mg cm^{-2}) was drop coated on the surface of the RDE (0.0706 cm^2) and 10 μL on the RRDE (0.2646 cm^2) electrode. The RRDE electrode is made up of a glassy carbon (GC) disk (diameter = 6 mm) and a Pt ring (outer diameter = 9 mm, and inner diameter = 7.5 mm). After coating the material evenly, the electrode was dried under an IR-lamp for 1 h. In this way, the working electrode was prepared for the electrochemical study.

An aqueous 1 M KOH solution (de-aerated with nitrogen gas) was used as an electrolyte for both the RDE and RRDE studies. All the electrode potentials reported in our work were first converted into the reversible hydrogen electrode (RHE) through a RHE calibration experiment (**Figure S19**), and for 1 M KOH, $\mathbf{E_{(RHE)} = E_{(Hg/HgO)} + 0.917\ V}$. All the RDE and RRDE analysis were carried out at a constant rotating rate of 1600 rpm in order to maintain uniform ionic concentration of the reactant and also to prevent accumulation of the products, *i.e.,* O_2 bubbles in the present case.

The entire linear sweep voltammetry data was corrected with 85% *iR*-compensation, where *i* and *R* indicate the current measured and the ohmic resistance generated between the working and reference electrode, respectively. In our study, for the catalyst coated electrode, ohmic resistance *R* of the whole electrochemical cell was determine using ZIR technique with a single point high frequency impedance measurement at 100 KHz with 20 mV amplitude about OCV. And *R* value is found to be 15.5 Ω, while in case of bare RDE, *R* was found to be in the region of 15–20 Ω. Current densities were normalized using electrode surface area and the reaction overpotential was determined using the equation: $\eta = [E_{(RHE)} - 1.23]$ V.

The Faradaic impedance using PEIS technique (Potentio Electrochemical Impedance Spectroscopy) was performed by using a SP-300 Biologic test station in the Faradaic region at 1.54 V *vs.* RHE covering the 5 mHz–100 kHz frequency range with 10 mV amplitude of sinusoidal potential perturbation as followed by **J**.F.C. Boodts *et al.* to study the Faradaic impedance of oxygen evolution reaction.[3] Several PEIS measurements were performed; the first impedance measurement was done prior to any OER polarization experiment followed by the PEIS test after every 50 loops of LSV (in the potential window of 0.92 V to 1.62 V *vs.* RHE at a scan rate of 10 mV s^{-1}). The fitted Nyquist plots for the Faradaic impedance and the equivalent electrical circuit diagram are given in **Figure S16 (a)** and **(b),** respectively. All the impedance values are normalized with the electrode area of 0.0706 cm^2.

RRDE technique was employed to confirm the oxygen evolution by the catalyst coated on the disk and the faradaic efficiency was determined by the collection of dissolved O_2 produced at the surrounding Pt-ring electrode. Prior to faradaic efficiency calculation experiment, the collection efficiency (N) of the RRDE electrode was determined using $K_3Fe(CN)_6$ in 1 M KCl solution by cyclic voltammetry and the calculated N value is 0.37.

Calculation method:

A calculation for the faradaic efficiency of the electrocatalyst is summarized below:

First, we have determined the collection efficiency ($N_{empirical}$) of the RRDE using the following equation:

$$N_{empirical} = I_r/I_d \tag{S1}$$

Where,

I_r = limiting current of ring electrode

I_d = limiting current of disk electrode.

Subsequently, the faradaic efficiency (ε) has been calculated using the following equation:

$$\varepsilon = 2 * I_r/I_d * N_{empirical} \tag{S2}$$

4. Results:

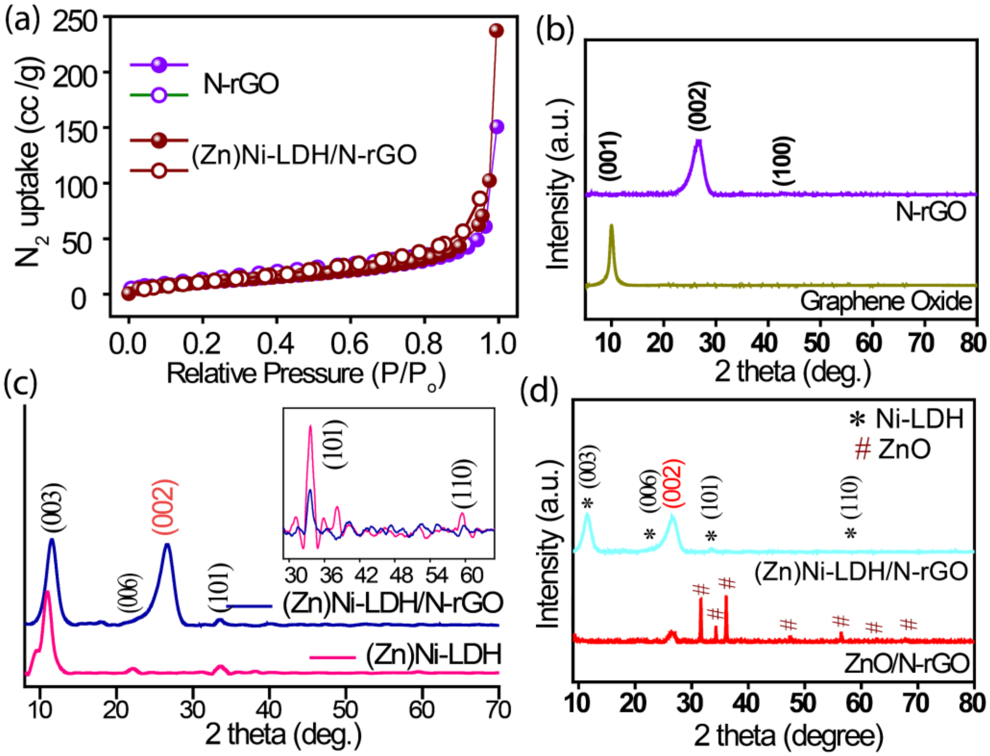

Figure S1: (a) *N_2 adsorption-desorption isotherms of N-rGO and (Zn)Ni-LDH/N-rGO, (b) comparative PXRD patterns of GO and N-rGO, (c) comparative PXRD patterns of (Zn)Ni-LDH/N-rGO and unsupported (Zn)Ni-LDH where the inset shows the poorly intense (101) and (110) planes, (d) comparative PXRD pattern of (Zn)Ni-LDH/N-rGO and ZnO/N-rGO.*

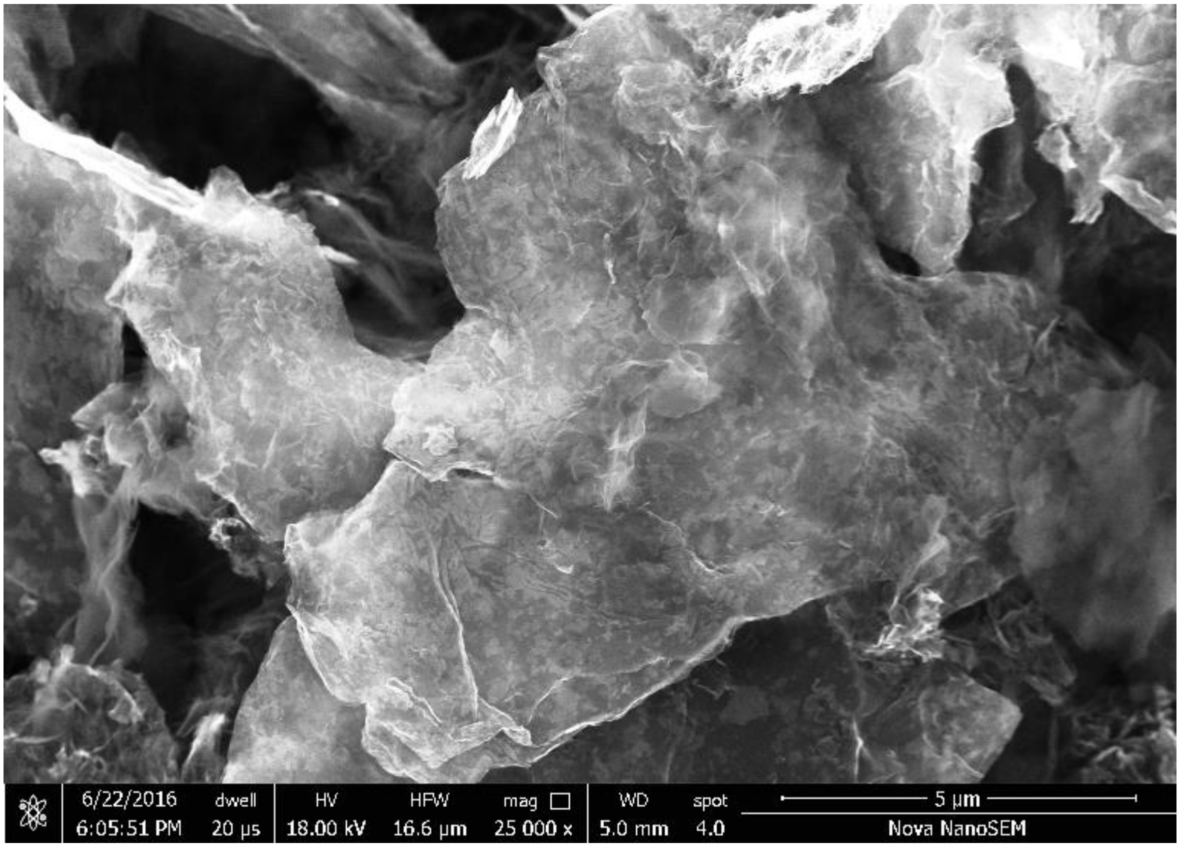

Figure S2: *FESEM image of (Zn)Ni–LDH/N-rGO indicating clear micro-sized LDH-patches anchored over large N-rGO sheets.*

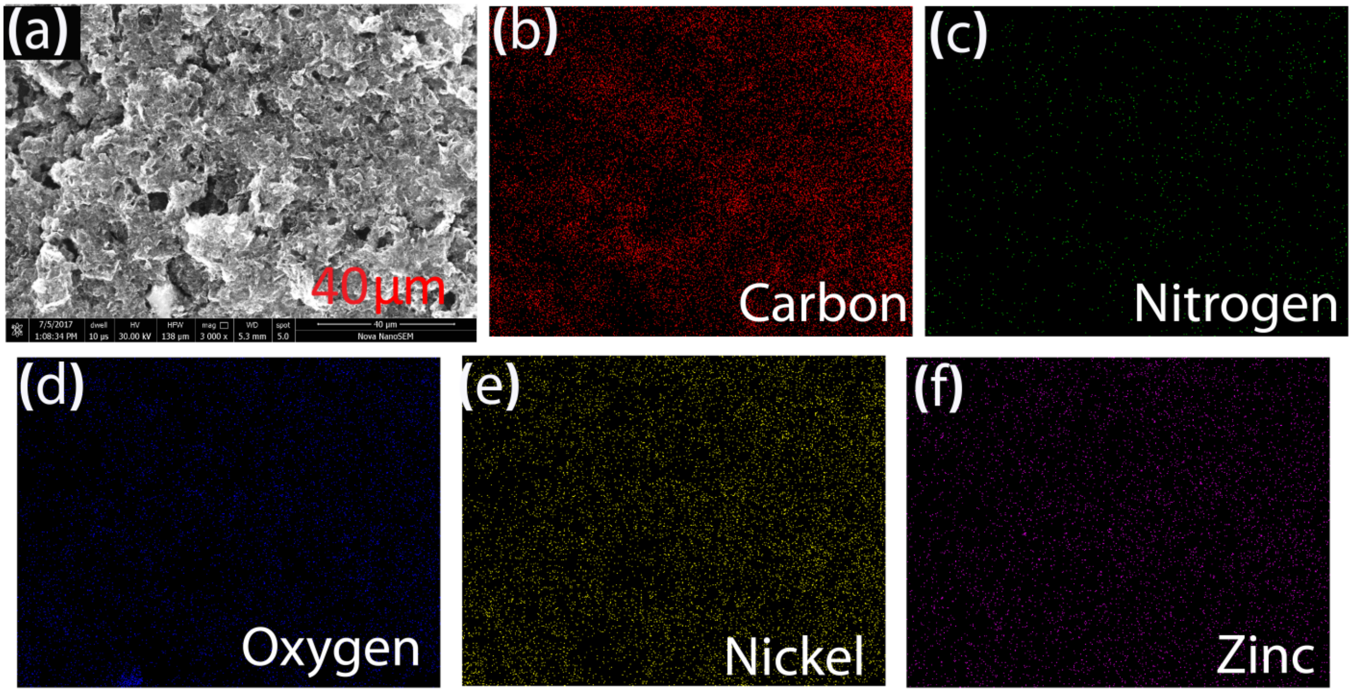

Figure S3: *FESEM elemental mapping of (Zn)Ni-LDH/N-rGO, (a) SEM image selected for the FESEM elemental mapping, (b) carbon, (c) nitrogen, (d) oxygen, (e) nickel and (f) zinc elemental mapping images.*

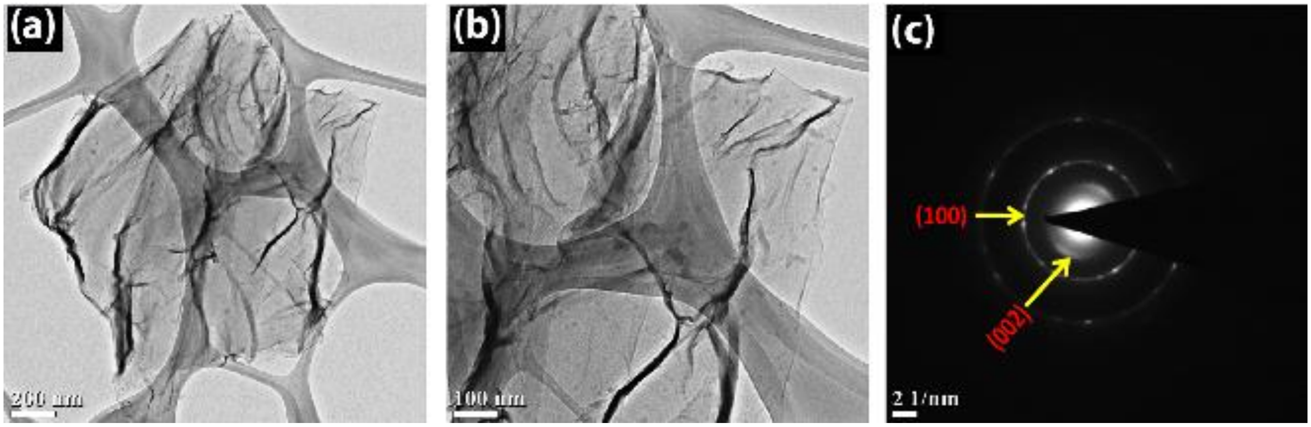

Figure S4: *TEM images of N-rGO, (a) and (b) the TEM images at different magnifications and (c) SAED pattern exhibiting clear N-rGO planes.*

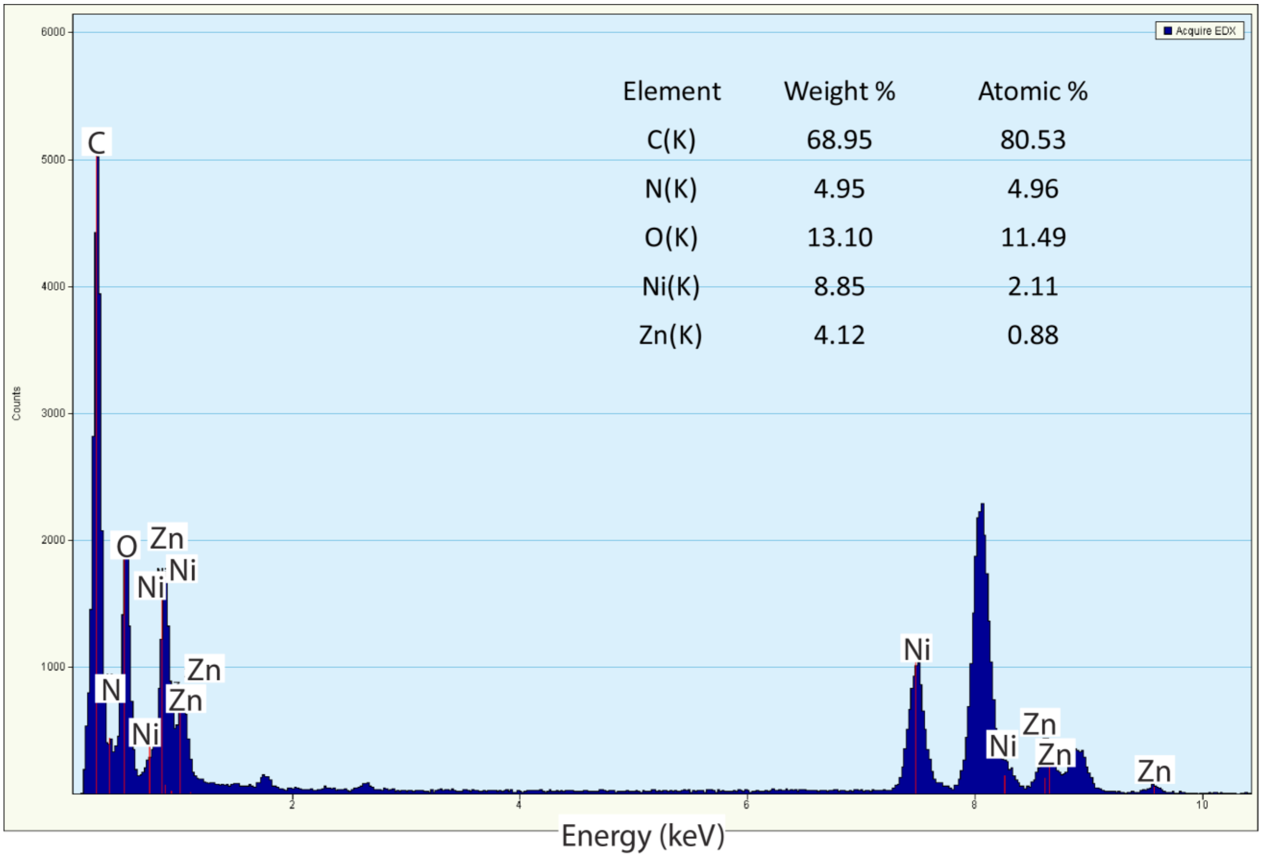

Element	Weight %	Atomic %
C(K)	68.95	80.53
N(K)	4.95	4.96
O(K)	13.10	11.49
Ni(K)	8.85	2.11
Zn(K)	4.12	0.88

Figure S5. *TEM-EDS spectrum of (Zn)Ni-LDH/N-rGO.*

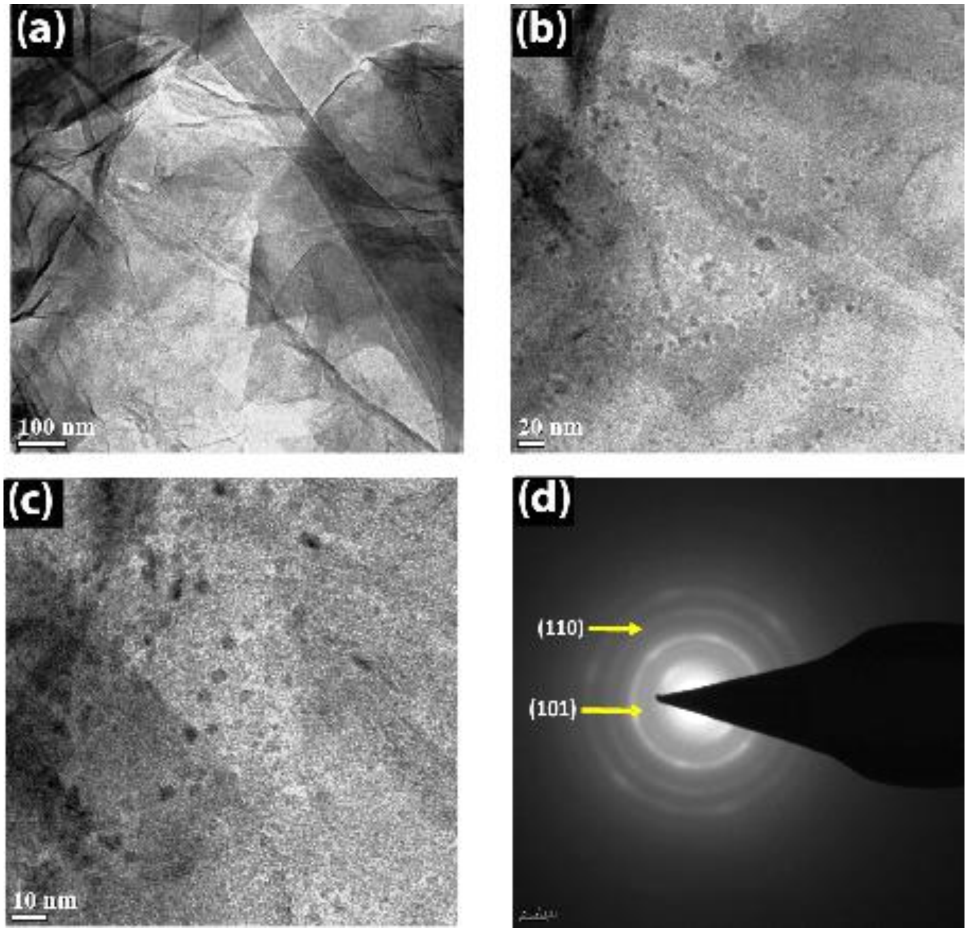

Figure S6: *TEM images of α-Ni(OH)$_x$/N-rGO, (a) the presence of thin crumbled hydroxide layers over N-rGO, (b) TEM image at higher magnification, (c) the embedded Ni nanoparticles (Ni-NPs) and (d) the corresponding SAED pattern revealing the α-Ni(OH)$_2$ diffraction planes.*

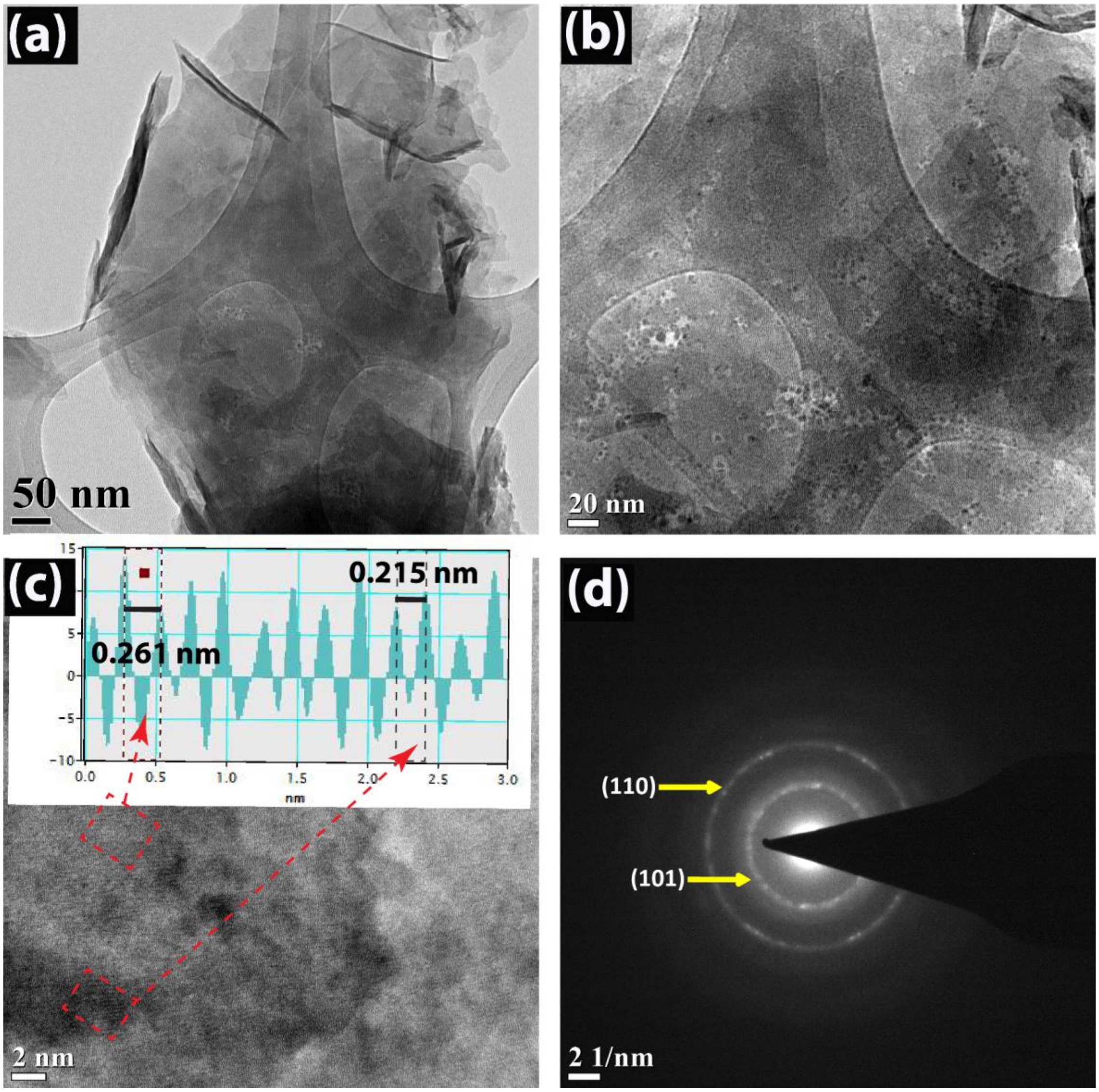

Figure S7: *TEM images of the unsupported (Zn)Ni-LDH, (a) the TEM image having thick patch like structure, (b) the hydroxide layer covered mono-dispersed NPs, (c) the ill-defined α-NiZn NPs with LDH layers, and d-spacing is found to be different in different region shown by red dotted box (i.e., 0.261 nm corresponding to LDHs and 0.215 nm corresponding to α-NiZn NPs) and (d) the SAED pattern with the characteristic LDHs planes.*

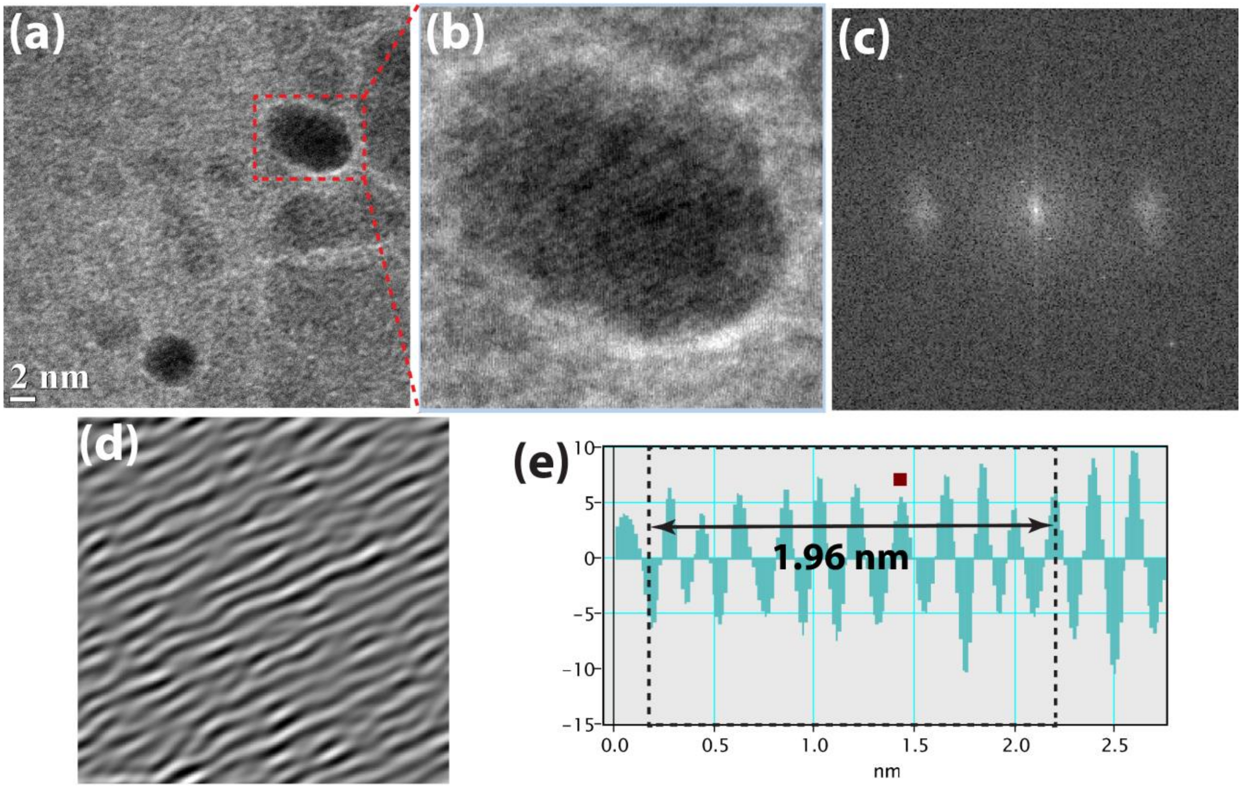

Figure S8: *(a) High magnification TEM image, (b) Inverse FFT (IFFT) of Reduced FFT, (c) fast Fourier transform image (FFT), (d) IFFT pattern and (e) profile of IFFT pattern of (Zn)Ni-LDH/N-rGO.*

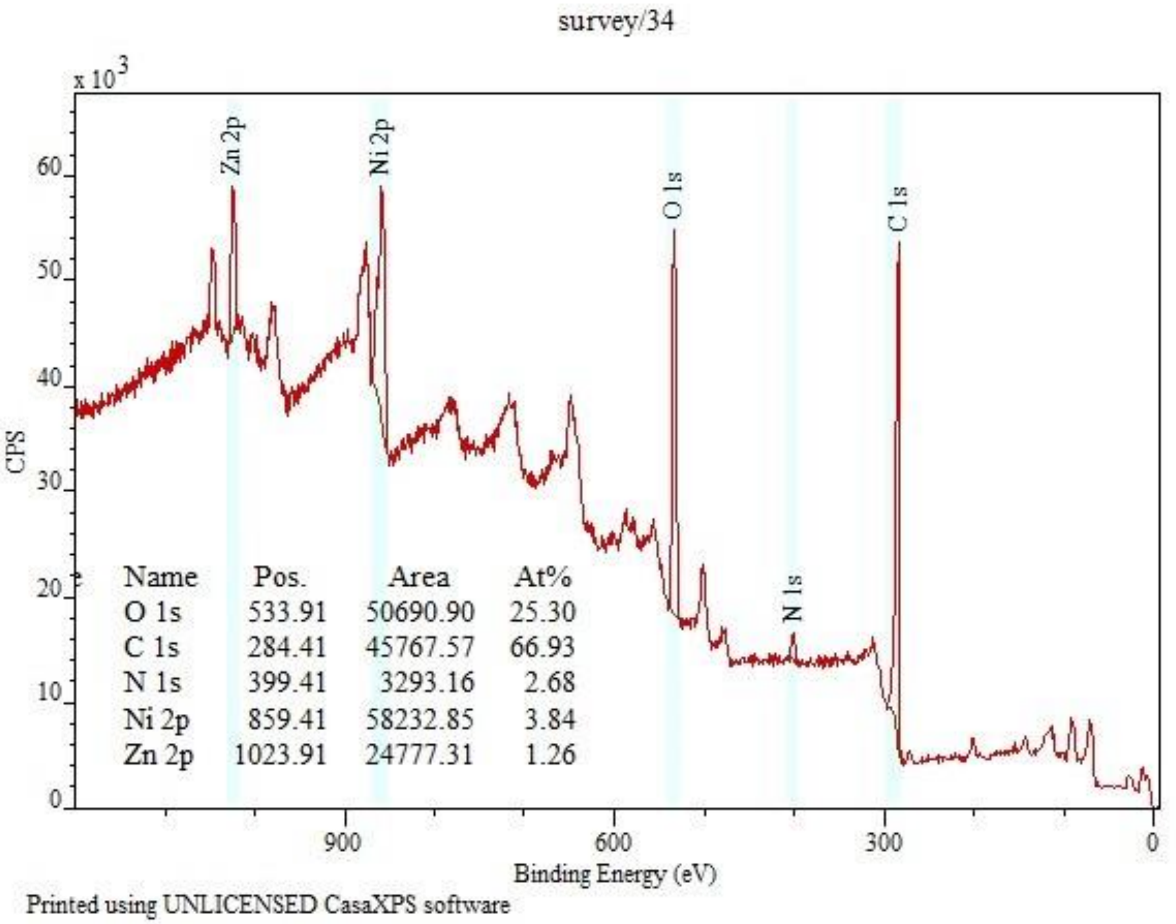

Name	Pos.	Area	At%
O 1s	533.91	50690.90	25.30
C 1s	284.41	45767.57	66.93
N 1s	399.41	3293.16	2.68
Ni 2p	859.41	58232.85	3.84
Zn 2p	1023.91	24777.31	1.26

Figure S9: *XPS survey spectrum of (Zn)Ni-LDH/N-rGO showing the atomic percentages of the different elements present in the system as determined through CASAXPS software.*

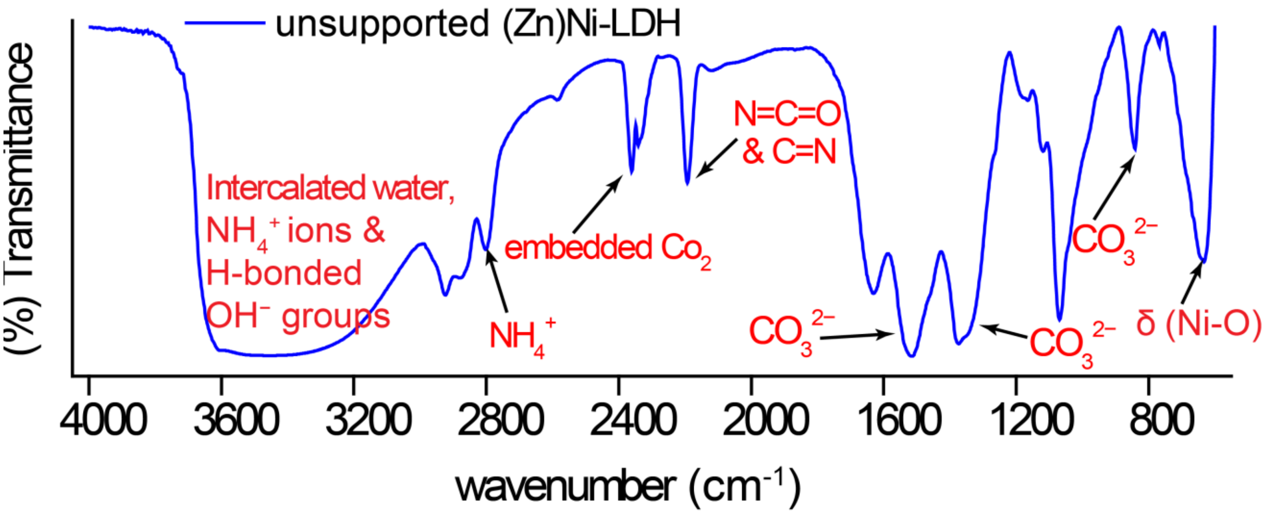

Figure S10. *FTIR spectrum of the unsupported (Zn)Ni-LDH.*

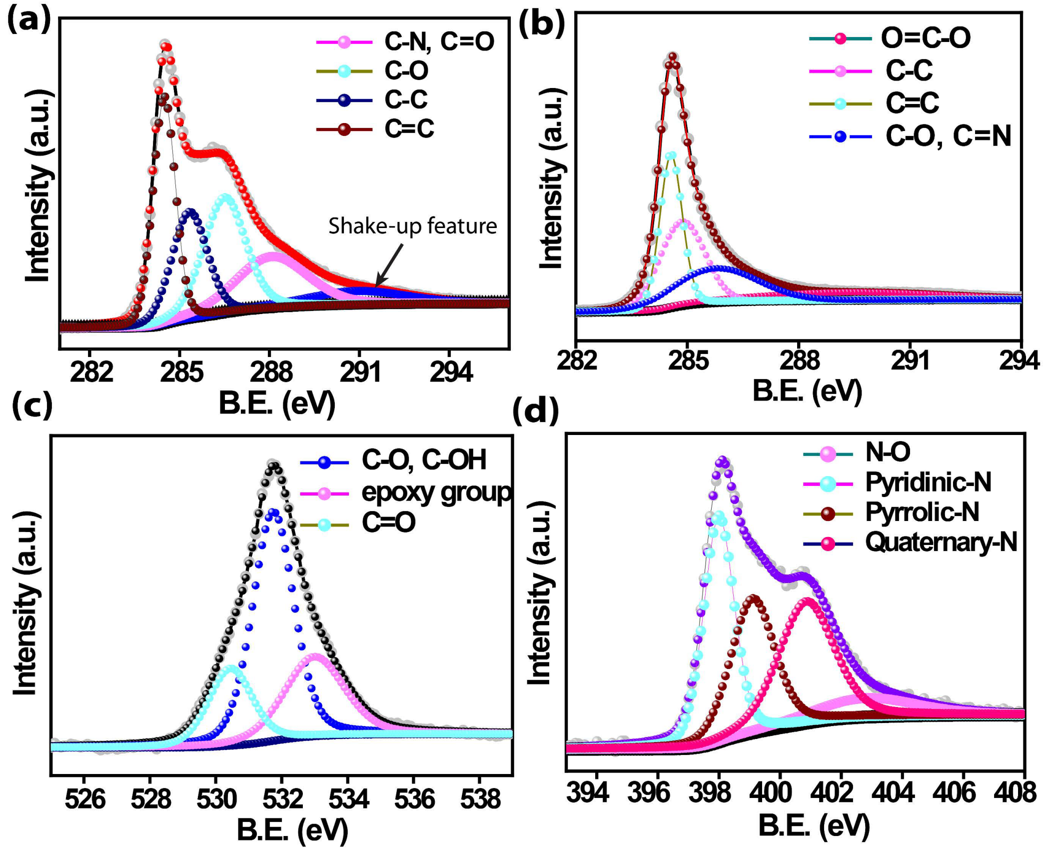

Figure S11: *Deconvoluted XPS spectra: (a) C1s of (Zn)Ni–LDH/N-rGO, (b) C1s of N-rGO, (c) O1s of N-rGO and (d) N1s of N-rGO.*

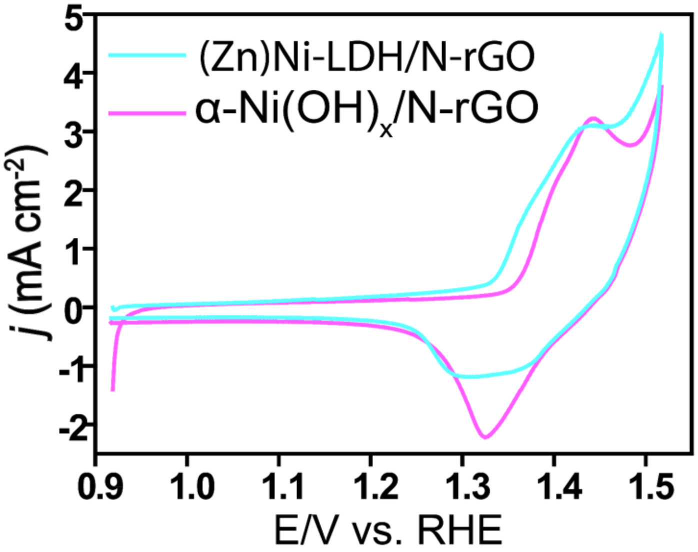

Figure S12: *Comparative cyclic voltammograms (1*st *cycle) of (Zn)Ni-LDH/N-rGO and α-Ni(OH)*$_{x}$*/N-rGO.*

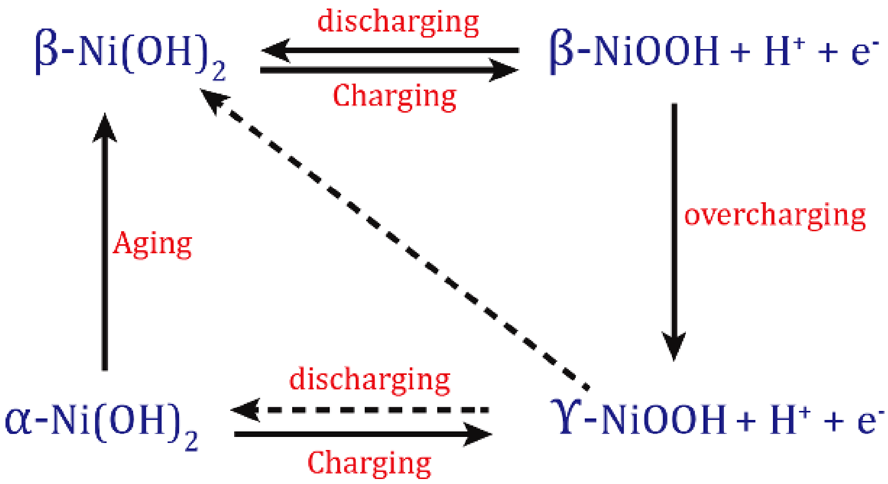

Figure S13: *Bode scheme representing the general chemical and electrochemical processes that occur during the water oxidation reaction on the nickel hydroxide electrode.*[4]

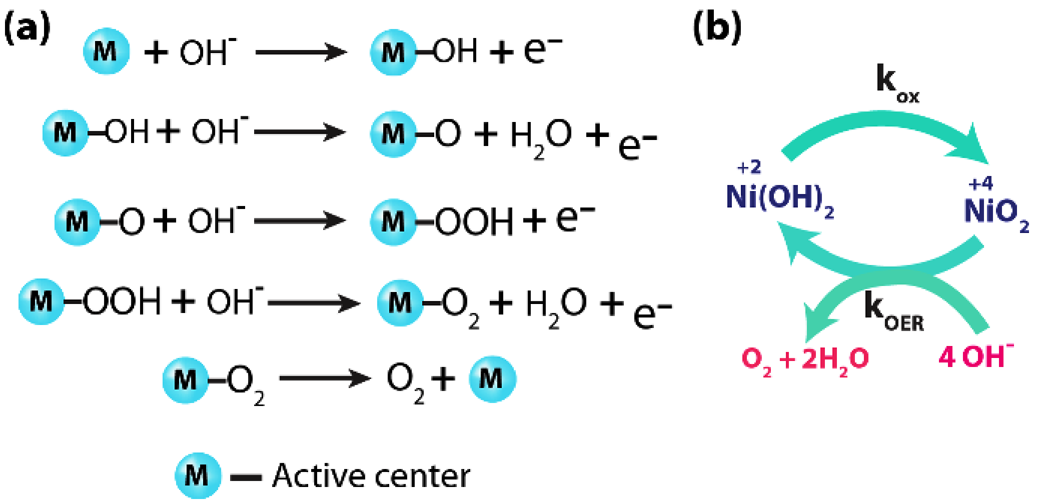

Figure S14: *(a) OER mechanism in alkaline medium,*[5] *(b) a general electrochemical water oxidation cycle over the* $Ni(OH)_2$ *based electrocatalyst with the nickel oxidation rate constant (*k_{ox}*) and OER rate constant (*k_{OER}*).*[6]

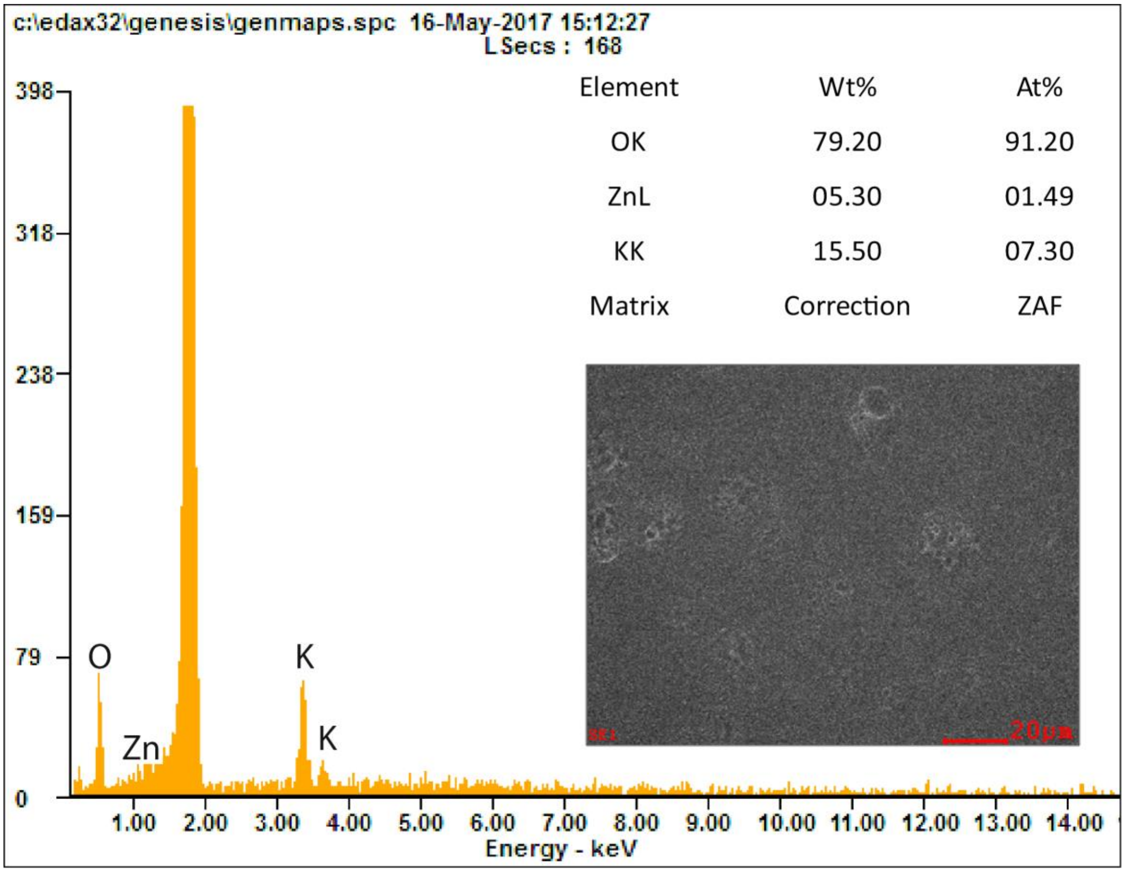

Element	Wt%	At%
OK	79.20	91.20
ZnL	05.30	01.49
KK	15.50	07.30
Matrix	Correction	ZAF

Figure S15. *FESEM-EDS spectrum of the electrolyte collected after the stability test to detect the presence of dissolved Zn. Inset exhibits the EDS table and SEM image.*

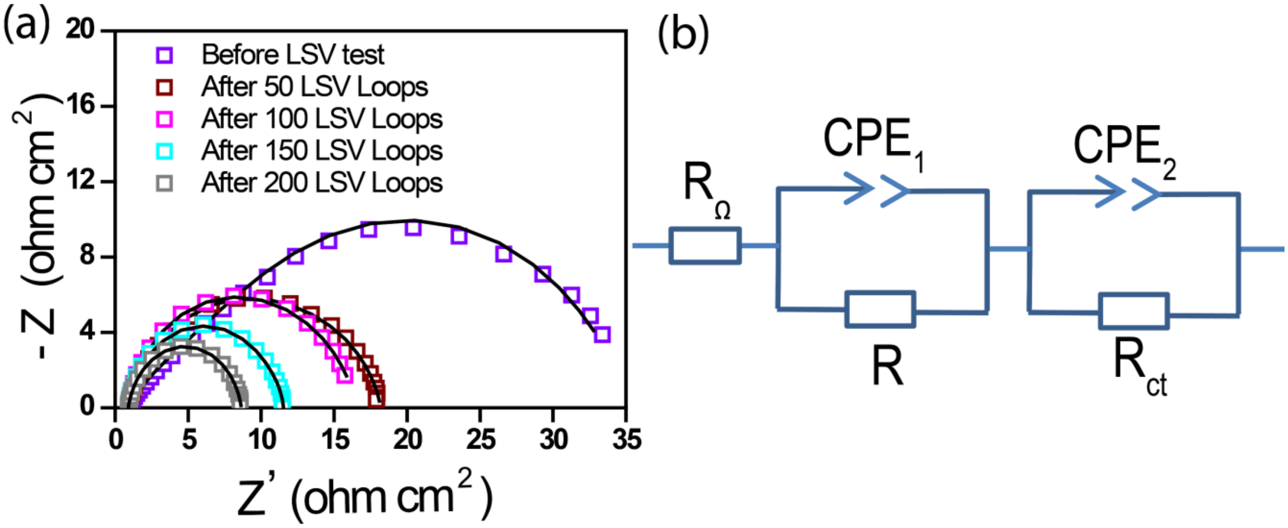

Figure S16. *(a) The fitted Faradaic impedance spectra in the Nyquist form of (Zn)Ni-LDH/N-rGO in 1 M KOH at 1.54 V vs. RHE before and after the different LSV loops; (b) the equivalent circuit used in the analysis of the experimental EIS data, where* R_Ω *refers to the ohmic resistance, parallel R-*CPE_1 *is attributed to the electrode surface geometry whereas the symbols* R_{ct} *and* CPE_2 *are indicating the charge transfer resistance and constant phase element corresponding to double-layer capacitance (*C_{dl}*), respectively.*

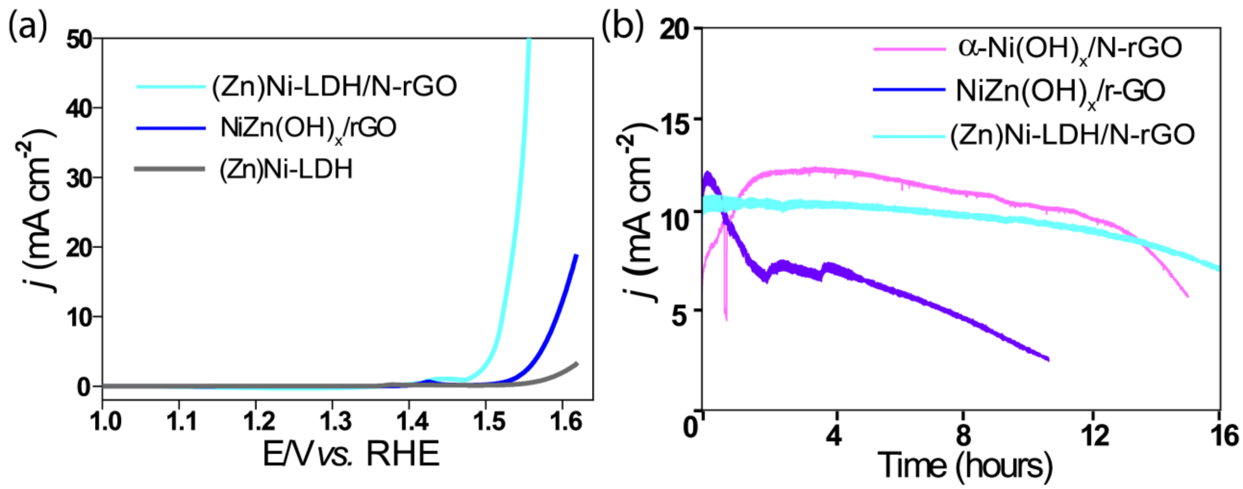

Figure S17: *(a) Comparative linear sweep voltammograms of (Zn)Ni-LDH/N-rGO, NiZn(OH)$_x$/rGO and unsupported (Zn)Ni-LDH, (b) Comparative chronoamperometric profiles of (Zn)Ni-LDH/N-rGO, NiZn(OH)$_x$/rGO and α-Ni(OH)$_x$/N-rGO.*

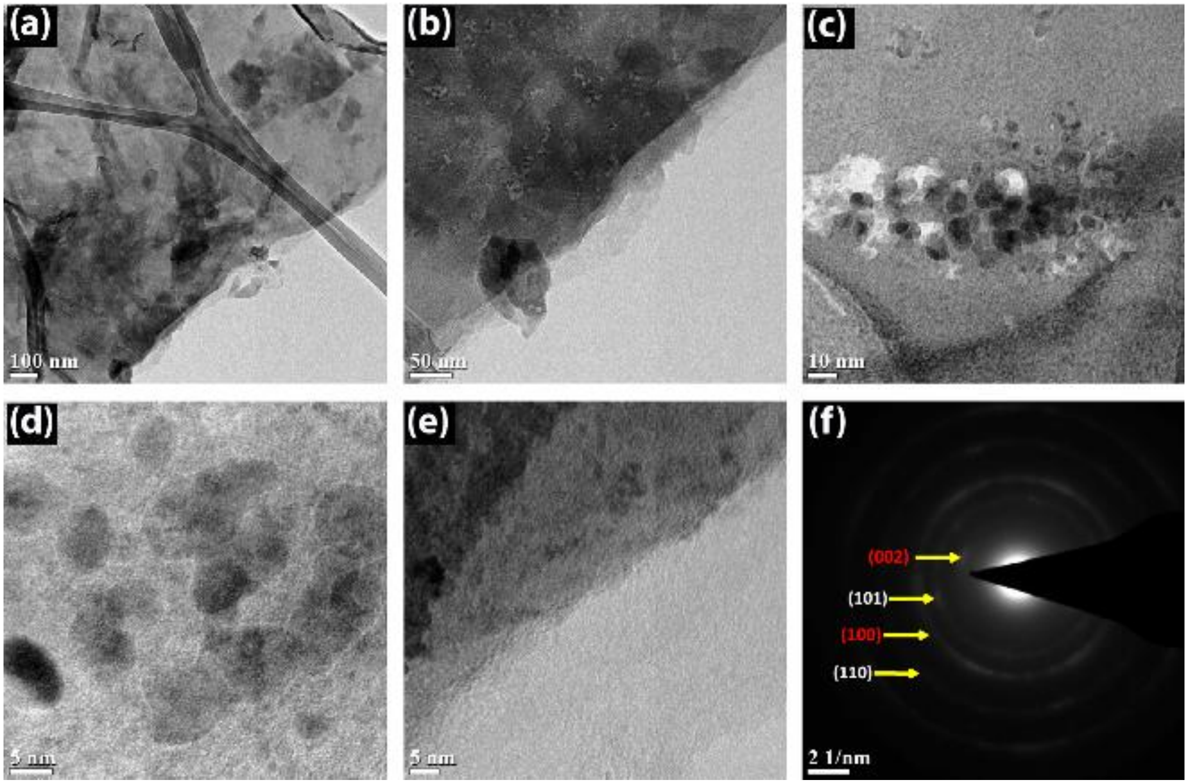

Figure S18: *TEM images of (Zn)Ni-LDH/N-rGO after chronoamperometry: (a), (b) and (c) represent the TEM images at different magnifications, (d) represents the high resolution TEM* *images revealing the ill-defined and deformed NPs, (e) represents the LDHs anchored over N-rGO sheets and (f) SAED pattern exhibiting both LDH (white) and N-rGO (red) planes.*

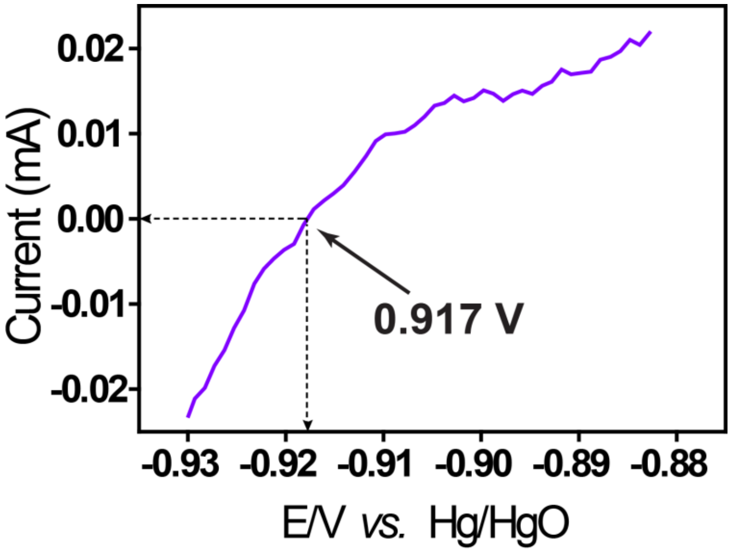

Figure S19: *(a) LSV for Hg/HgO to RHE calibration in 1M KOH.*

***Table S1**: Comparison of the OER activity data for the different synthesized catalysts.*

Sr.No.	**Electrocatalyst**	**Overpotential (mV)**	**Tafel slope (mV/dec.)**
1.	(Zn)Ni-LDH/N-rGO	290	44
2.	$Ni(OH)_x$/N-rGO	330	52
3.	$NiZn(OH)_x$/N-rGO	360	74
4.	20% RuO_2/C	306	--

***Table S2**: Comparison of the OER activity data of the present work with the different works published in the literature.*

Sr. No.	Electrocatalyst	Overpotential (mV)	Electrolyte	Tafel slope (mV/dec.)	Catalyst loading (mg/cm^2)	Ref.
1.	α- $Ni(OH)_2$ spheres	331	0.1 M KOH	42	0.2	7
2.	ZnCo-LDH/rGO	330	0.1 M KOH	73	0.25	8
3.	$ZnCo_2O_4$/NCNT	420	0.1 M KOH	70.6	0.2	9
4.	Porous NiFe-oxide	328	0.1 M KOH	42	0.143	10
5.	NiCo-binary oxide	325	1 M NaOH	39	---	11
6.	N-Graphene	380	0.1 M KOH	---	0.2	12
7.	Ni/N/C	390	0.1 M KOH	44	---	13
8.	(Zn) Ni-LDH/N-rGO	290	1 M KOH	44	0.18	Present Work
9.	IrO_2	470 mV	1 M KOH	61	0.14	14
10.	IrO_2	350	0.1 M KOH	55	0.4	15
11.	Commercial 20%-Ru/C	390	0.1 M KOH	---	0.028	16
12.	Commercial 20%-Ir/C	380	0.1 M KOH	---	0.028	16

References:

1. D. C. Marcano, D. V. Kosynkin, J. M. Berlin, A. Sinitskii, Z. Sun, A. Slesarev, L. B. Alemany, W. Lu and J. M. Tour, *ACS Nano*, 2010, **4**, 4806-4814.
2. T. Audichon, T. W. Napporn, C. Canaff, C. Morais, C. Comminges and K. B. Kokoh, *J. Phys. Chem. C*, 2016, **120**, 2562-2573.
3. V. A. Alves, L. A. da Silva and J. F. C. Boodts, *Electrochimica Acta*, 1998, **44**, 1525-1534.
4. D. S. Hall, D. J. Lockwood, C. Bock and B. R. MacDougall, *P ROY SOC A-MATH PHY*, 2015, **471**.

5. V. M. Dhavale, S. S. Gaikwad, L. George, R. N. Devi and S. Kurungot, *Nanoscale*, 2014, **6**, 13179-13187.
6. M. Görlin, P. Chernev, J. Ferreira de Araújo, T. Reier, S. Dresp, B. Paul, R. Krähnert, H. Dau and P. Strasser, *J. Am. Chem. Soc.*, 2016, **138**, 5603-5614.
7. M. Gao, W. Sheng, Z. Zhuang, Q. Fang, S. Gu, J. Jiang and Y. Yan, *J. Am. Chem. Soc.*, 2014, **136**, 7077-7084.
8. D. Tang, Y. Han, W. Ji, S. Qiao, X. Zhou, R. Liu, X. Han, H. Huang, Y. Liu and Z. Kang, *Dalton Trans*, 2014, **43**, 15119-15125.
9. Z.-Q. Liu, H. Cheng, N. Li, T. Y. Ma and Y.-Z. Su, *Adv. Mater.*, 2016, **28**, 3777-3784.
10. J. Qi, W. Zhang, R. Xiang, K. Liu, H.-Y. Wang, M. Chen, Y. Han and R. Cao, *Adv. Sci.*, 2015, **2**, 1500199-n/a.
11. Y. Yang, H. Fei, G. Ruan, C. Xiang and J. M. Tour, *ACS Nano*, 2014, **8**, 9518-9523.
12. Y. Zhao, R. Nakamura, K. Kamiya, S. Nakanishi and K. Hashimoto, *Nat. Commun.*, 2013, **4**, 2390.
13. J. Ren, M. Antonietti and T.-P. Fellinger, *Adv. Energy Mater.*, 2015, **5**, 1401660-n/a.
14. X. Yu, M. Zhang, W. Yuan and G. Shi, *J. Mater. Chem. A*, 2015, **3**, 6921-6928.
15. J. Ren, M. Antonietti and T.-P. Fellinger, *Adv. Energy Mater.*, 2015, **5**, n/a-n/a.
16. Y. Gorlin and T. F. Jaramillo, *J. Am. Chem. Soc.*, 2010, **132**, 13612-13614.